Lattice Dynamics of Zeolitic Silica Polymorphs

A. J. M. de Man,[†] B. W. H. van Beest,[‡] M. Leslie,[§] and R. A. van Santen*,[†,‡]

*Laboratory of Inorganic Chemistry and Catalysis, Eindhoven University of Technology, P.O. Box 513,
5600 MB Eindhoven, The Netherlands, Koninklijke/Shell-Laboratorium Amsterdam (Shell Research B.V.),
P.O. Box 3003, 1003 AA Amsterdam, The Netherlands, and SERC SRS Laboratory, Daresbury,
Warrington WA4 4AD, United Kingdom (Received: January 17, 1989; In Final Form: June 14, 1989)*

Rigid ion and shell model calculations of the infrared and Raman active modes of α-quartz, aluminum-free sodalite, and dealuminated faujasite are presented. Results of the rigid ion calculations show poor agreement with experimental data but the agreement significantly improved when using shell model calculations. A group theoretical analysis of the spectra enables an analysis in terms of dominantly stretching, bending, or torsional modes. A rather good agreement of the frequencies in the bending and torsional mode regions is found. One concludes from comparing with the stretching modes that the short range potential for the Si–O stretch frequency is too weak. The improvement of the shell model versus the rigid ion model results can be ascribed to screening of the long range electrostatic interactions by polarization of the O^{2-} anions. Calculated frequency splittings between transversal and longitudinal optical modes indicate that the use of partial ionic charges, in combination with an improved short range potential, might result in a better simulation of the infrared and Raman spectra.

Introduction

Insight into the factors that govern the relative stability of zeolites as a function of both lattice topology and composition is of relevance to the physical chemistry of zeolite synthesis.[1] Theoretical approaches to this problem can be distinguished into two types.

In the first approach representative parts of the zeolite lattice are isolated, e.g. rings or cages, and quantum mechanical ab initio[2-6] or semiempirical techniques[6-10] are used to compute the conformation or relative stabilities of such clusters. Complete crystallographic unit cells of zeolites are usually too large to be calculated on this level.

The other approach is to employ infinite lattice techniques using electrostatic (two-body) potentials. The energies can be derived immediately from Madelung potentials,[11] but the usual approach is to minimize the lattice energy by relaxing the structure.[12] In addition to the long-range electrostatic potential, short-range classical interatomic potentials fitted on the structure and elasticity constants[1,13-15] are used.

Pure valence force field calculations have been applied too,[16-18] and a combination of valence force fields and electrostatic forces has recently been used to simulate an isolated sodalite cage.[19]

In particular α-quartz has been studied thoroughly by using pure valence force field models (nearest neighbor and next nearest neighbor interactions),[20-23] potentials consisting of a (long range) electrostatic term and a short range interaction,[14,22-24] and even a pure electrostatic model.[25] Potentials developed for α-quartz[14] have recently been used to predict the structures of aluminum-free zeolitic silica polymorphs.[13,15]

The purpose of the work reported here is to investigate the applicability of the potentials used more closely via comparison of calculated and measured infrared and Raman spectra for a few structures.

The results of rigid ion and shell model calculations are presented for α-quartz, aluminum-free sodalite, and aluminum-free faujasite. Calculated infrared and Raman spectra for the three compounds are compared with experimental data on high-silica or dealuminated samples. Computed lattice energies will also be presented.

It will appear that this approach yields valuable insights into the quality of the potentials used and provides indications in which direction further improvements of the potentials have to be sought.

Methods and Models

Bonding in SiO_2 is assumed to have a large ionic component, so the potential used consists of a long-range electrostatic term and a short-range covalent term. The long-range term is calculated by using an Ewald summation of the Coulomb term between point charges.

The short-range potential that is employed here is of a Buckingham[26] type $V_{ij}{}^s$ (with a Born repulsion term and a van der

(1) Ooms, G.; van Santen, R. A.; den Ouden, C. J. J.; Jackson, R. A.; Catlow, C. R. A. *J. Phys. Chem.* **1988**, *92*, 4462.

(2) Newton, M. D.; O'Keeffe, M.; Gibbs, G. V. *Phys. Chem. Miner.* **1980**, *6*, 305.

(3) van Beest, B. W. H.; Verbeek, J.; van Santen, R. A. *Catal. Lett.* **1988**, *1*, 147.

(4) Fripiat, J. G.; Berger-André, F.; André, J.; Derouane, E. G. *Zeolites* **1983**, *3*, 306.

(5) Sauer, J.; Zahradnik, R. *Int. J. Quantum Chem.* **1984**, *26*, 793. Sauer, J. *J. Phys. Chem.* **1987**, *91*, 2315.

(6) Pelmenshchikov, A. G.; Paukshtis, E. A.; Stepanov, V. S.; Ione, K. G.; Zhidomirov, G. M.; Zamaraev, K. I. *Proc. Int. Congr. Catal., 9th* **1988**, *1*, 404.

(7) Zhidomirov, G.; Kazansky, V. *Adv. Catal.* **1986**, *34*, 131.

(8) Ooms, G.; van Santen, R. A. *Recl. Trav. Chim. Pays-Bas* **1987**, *106*, 69.

(9) Beran, S.; Jírů, P.; Wichterlová, B. *J. Phys. Chem.* **1981**, *85*, 1951. Beran, S. *J. Phys. Chem.* **1981**, *85*, 1956. Beran, S.; Jírů, P.; Wichterlová, B. *React. Kinet. Catal. Lett.* **1981**, *18*, 51–53. Beran, S. *J. Phys. Chem.* **1982**, *86*, 111. Beran, S. *Chem. Phys. Lett.* **1982**, *91*, 86. Beran, S. *Z. Phys. Chem. (Munich)* **1982**, *130*, 81. Beran, S. *Z. Phys. Chem. (Munich)* **1983**, *137*, 89.

(10) Mortier, W. J.; Geerlings, P.; van Alsenoy, C.; Figeys, H. P. *J. Phys. Chem.* **1979**, *83*, 3257.

(11) Dempsey, E. *J. Phys. Chem.* **1969**, *75*, 3660.

(12) Catlow, C. R. A.; Mackrodt, W. C. *Computer Simulation of Solids, Lecture Notes on Physics*; Springer: Vienna, 1982. Catlow, C. R. A.; Doherty, M.; Price, G. D.; Sanders, M. J.; Parker, S. C. *Mater. Sci. Forum* **1986**, *7*, 163–175.

(13) Ooms, G.; van Santen, R. A.; Jackson, R. A.; Catlow, C. R. A. *Stud. Surf. Sci. Catal.* **1988**, *37*, 317.

(14) Sanders, M. J. *Computer Simulation of Framework Structured Minerals*, Ph.D. Thesis, University of London, 1984.

(15) Jackson, R. A. *Mol. Simulation* **1987**, *2*.

(16) Blackwell, C. S. *J. Phys. Chem.* **1979**, *83*, 3251. Blackwell, C. S. *J. Phys. Chem.* **1979**, *83*, 3257.

(17) Demontis, P.; Suffritti, G. B.; Quartieri, S.; Fois, E. S.; Gamba, A. *Zeolites* **1987**, *7*, 522. Demontis, P.; Suffritti, G. B.; Quartieri, S.; Fois, E. S.; Gamba, A. *J. Phys. Chem.* **1988**, *92*, 867.

(18) No, K. T.; Bae, D. H.; Jhon, M. S. *J. Phys. Chem.* **1986**, *90*, 1772.

(19) Mabilia, M.; Pearlstein, R. A.; Hopfinger, A. J. *J. Am. Chem. Soc.* **1987**, *109*, 7960.

(20) Kleinman, D. A.; Spitzer, W. G. *Phys. Rev.* **1962**, *125*, 16.

(21) Etchepare, J.; Marian, M. *J. Chem. Phys.* **1974**, *60*, 1873.

(22) Elcombe, M. M. *Proc. Phys. Soc.* **1967**, *91*, 946.

(23) Barron, T. H. K.; Huang, C. C.; Pasternak, A. *J. Phys. C* **1976**, *9*, 3925.

(24) Striefler, M. E.; Barsch, G. R. *Phys. Rev. B* **1975**, *12*, 4553.

(25) Brunner, G. O. *Phys. Chem. Miner.* **1984**, *10*, 273.

† Eindhoven University of Technology.
‡ Koninklijke/Shell-Laboratorium Amsterdam.
§ SERC SRS Laboratory.

Waals attraction term, formula 1) in combination with a harmonic

$$V_{ij}{}^{s} = A_{ij} \exp\left(\frac{-r_{ij}}{\rho}\right) - \frac{C_{ij}}{r_{ij}{}^{6}} \tag{1}$$

bond bending (three-body) term V_{hij} (formula 2), where r_{ij} is the distance between atom i and j and A_{ij}, ρ_{ij}, and C_{ij} are short-range parameters. The three-body term is

$$V_{hij} = -k_{hij}(\theta_{hij} - \theta^{\circ}{}_{hij})^2 \tag{2}$$

where k_{hij} is the (bending) force constant, θ_{hij} is the angle between the atoms h, i (central atom), and j, and $\theta^{\circ}{}_{hij}$ is the equilibrium value of θ_{hij}.

This approach promises a better transferability of the potential to other systems than the generally used force field models.[20-23] The model discussed so far is called the three-body rigid ion model. It can be extended to a model that accounts for ionic polarizabilities: the so-called shell model.[27] According to this model the ion is thought of as consisting of a core and a massless shell interconnected by a "spring". The shell has a charge Y and the core has a charge that is equal to $Z - Y$ where Z is the total ionic charge. Usually the spring is considered to be harmonic. The polarizability α of a free ion is then given by[12]

$$\alpha = (Ye)^2/4\pi\epsilon_0 K \tag{3}$$

where α is the ionic polarizability, Y is the shell charge, e is the unit charge, ϵ_0 is the vacuum permittivity, and K is the core-shell harmonic spring constant.

The Buckingham potential and the three-body potential are defined between shells and not between cores.

Both the three-body rigid ion model and the three-body shell model were used in this study for the simulation of vibrational spectra.

The first step in calculating these spectra is to obtain a set of potential parameters that can be transferred from one silica structure to another. These parameters are usually obtained from a least-squares fit to macroscopic observables derived from experiments.

The second step in calculating the spectra is to obtain a relaxed structure. This structure is found by changing the positions of the ions in one crystallographic unit cell, starting from an experimentally derived structure, in such a way that the cohesive energy of the system is minimized by using the interatomic potential found before. The relaxation is performed by the THBREL code (originating from the PLUTO code[12,14]) without any symmetry constraints on the structure and can be done in two ways: (a) leaving the unit cell dimensions constant (constant volume minimization). Only internal strains are minimized in this approach. External strains still can be relatively large. (b) allowing the unit cell dimensions to change too (the constant pressure minimization), minimizing both internal and external strains. In this work a constant pressure minimization procedure is used. In the case of a shell model both the core positions and the shell positions are changed independently. The THBREL code also generates observables such as elastic constants, dielectric constants, and the lattice energy.

The third step in calculating the spectra is the generation of a phonon spectrum using the relaxed structure and the interatomic potential. This is done in the harmonic approximation by the THBPHON code,[28] which generates both the frequencies and the atom displacement vectors of the vibrational modes by diagonalizing the dynamical matrix of the system without any use of symmetry properties.

The last step is to derive the infrared and Raman spectra from the vibrational modes. First the modes are divided in infrared

active, Raman active, and inactive modes using a group theoretical projection method.[29] Then the infrared and Raman spectral line intensities are calculated. Intensities are very sensitive to the atomic displacement vectors, so they provide a check of eigenvectors, and they can be very useful when comparing the frequencies of calculated lines with experimental spectra because a lot of group theoretically active modes have a low intensity and hence do not show up in the actual spectrum.

The infrared line intensities are calculated by using the method of Kleinman and Spitzer.[20] An effective charge tensor $\mathbf{B}^i$ for every atom i in the crystallographic unit cell is defined

$$\mathbf{B}^i = q^i\mathbf{I} - Q^i\sum_j{}^{i}r^{ij}r^{ij} \tag{4}$$

where q^i is the ionic charge of atom i, $\mathbf{I}$ is the unit tensor, Q^i is the covalent charge of atom i, r^{ij} is the unit vector from i to j, and $\sum_j{}^{i}$ is the sum over the nearest neighbors of atom i.

The intensity of an infrared active vibration with atomic Cartesian displacement vectors u^i is proportional to

$$\sum_i |\mathbf{B}^i u^i|^2 \tag{5}$$

Because of electrical neutrality the values of q^i and Q^i have to be chosen such that

$$\sum_i \mathbf{B}^i = 0 \tag{6}$$

The Raman intensities are also calculated by a method given by Kleinman and Spitzer[20] using the following approximation for the electric susceptibility tensor χ:

$$\chi = \sum_i\sum_j (r^{ij}\cdot u^i)r^{ij}r^{ij} \tag{7}$$

(with the same definitions as in formulas 4 and 5).

The Raman intensity is proportional to

$$1 + \frac{1}{\exp(\hbar\omega/kT)}|\chi E|^2 \tag{8}$$

where $\hbar$ is Planck's constant divided by 2π, ω is the (angular) frequency of the vibrational mode, T is the temperature, and E is the polarization vector of incident radiation. Spectra will be drawn as lines of zero line width although line widths of as large as 25 cm^{-1} are not unusual.[30]

Details of the Calculations

It is not necessary to use ions with a charge equal to the full formal value in the long-range electrostatic potential; on the contrary, Price and Parker[31] obtained a good simulation of Mg_2SiO_4 by using charges of the ions that were about half the formal charges. Also relatively simple nearest neighbor rigid ion models for α-quartz used charges that were less than half the formal values,[22-24] and quantum mechanical calculations[3,4,9,10] indicate the same by the Mulliken populations. A compilation of partial charges reported in the literature can be found in Table I. One notes the small values sometimes used in rigid ion calculations, a point we will return to later on.

In order to compare rigid ion and shell model results, we will only report in this paper the results of calculations with full formal charges.

The Buckingham potential is calculated for all silicon-oxygen and oxygen-oxygen pairs with a mutual distance less than 10 Å (for comparison, the nearest neighbor Si-O distance in α-quartz is 1.61 Å, the O-O distance is 2.6 Å and the Si-Si distance is 3.1 Å). Parker[32] has found that the contribution of the Si-Si interaction is negligible although O'Keeffe and Hyde[33] suggested

(26) Buckingham, R. A. *Proc. R. Soc. London* **1936**, *A168*, 264.
(27) Dick, B. G.; Overhauser, A. W. *Phys. Rev.* **1958**, *112*, 91.
(28) Dolling, G. Calculations of Phonon Frequencies. In *Methods in Computational Physics*; Gilat, G., Ed.; Academic Press: New York, 1976; Vol. 15.

(29) Maraduddin, A. A. *Theory of Lattice Dynamics in the Harmonic Approximation*; Academic Press: New York, 1971.
(30) Dowty, E. *Phys. Chem. Miner.* **1987**, *14*, 67.
(31) Price, G. D.; Parker, S. C. *Phys. Chem. Miner.* **1984**, *10*, 209.
(32) Parker, S. C. *Acta Crystallogr.* **1984**, *B40*, 200.
(33) O'Keeffe, M.; Hyde, G. *Acta Crystallogr.* **1978**, *B34*, 27.

TABLE I: Atomic Charges

ref	q^{Si}	q^O	model system	method
		Quantum Mechanical Calculations (Mulliken Populations)		
3	1.35	-0.69^a	$Si_3O_3(OH)_6$ ring	SCF STO3G
3	1.39	-0.71^a	$Si_4O_4(OH)_8$ ring	SCF STO3G
3	1.40	-0.72^a	$Si_5O_5(OH)_{10}$ ring	SCF STO3G
3	1.41	-0.72^a	$Si_6O_6(OH)_{12}$ ring	SCF STO3G
4	1.43	-0.64	$(OH)_3SiOSi(OH)_3$	LCAO-SCF-MO STO3G
9	1.66–1.74	-0.74 to -0.80	$Si_5O_5(OH)_{10}$ ring	CNDO/2(s,p)-basis
9	1.63–1.65	-0.67 to -0.75	$Si_6O_6(OH)_{12}$ ring	CNDO/2 (s,p)-basis
10	1.5931	-0.56 to -0.80	$Si_6O_6(OH)_{12}$ ring	CNDO (s,p)-basis
10	2.0605	-0.69 to -1.06	$Si_6O_6(OH)_{12}$ ring	CNDO/2 (s,p)-basis
		Fit on Vibrational Spectra		
22	1.94	-0.97	α-quartz	rigid ion model
23	0.694	-0.347	α-quartz	rigid ion model
24	0.944	-0.472	α-quartz	rigid ion model

^{a} For oxygen atom in the ring.

TABLE II: Three-Body Rigid Ion Potential Parameters[15]

	long range		two-body short range		three body	unit
	Si	O	Si–O	O–O	O–Si–O	
Z	+4.0	−2.0				e
A			1584.167	22764.3		eV
ρ			0.32962	0.149		Å
C			52.645	27.88		eV Å^6
θ°					109.47	deg
k					4.5815	eV/rad^2

TABLE III: Three-Body Shell Model Potential Parameters[35]

	long range		two-body short range		three body	shell	unit
	Si	O	Si–O	O–O	O–Si–O	core O	
Z	+4.0	−2.0					e
A			1283.907	22764.3			eV
ρ			0.32052	0.149			Å
C			10.66158	27.88			eV Å^6
θ°					109.47		deg
k					2.09724		eV/rad^2
Y						−2.86902	e
K						74.92	eV/Å^2

that silicates could be described by an Si–O and an Si–Si interaction, so neglecting the O–O potential.

The three-body interaction is only calculated between two Si–O bonds that share the same silicon atom in order to describe the tetrahedral unit properly.

The O–O short range repulsive interaction parameters used were derived from Hartree–Fock calculations by Catlow.[34] The parameters for the Si–O short range interaction, the three-body term, and the O–O van der Waals term were obtained[14,35] by fitting on the structure, elastic constants, and dielectric constants of α-quartz. The results of the fitting are given in Tables II and III. The potential parameters are the same as those used in ref 1, 15, 13, and 35.

Phonon calculations were performed by using a zero wave vector k having a length k of about 0.001 reciprocal lattice unit and pointing along the main symmetry axes. The frequencies of the optical modes for $k = 0$ are equal to those of the transversal optical modes for $k \neq 0$.

Infrared intensities will be presented using $Q^i = 0$ and q^i equal to the formal ionic charge for all ions (formula 4). Longitudinal modes are not included in the figures representing calculated infrared spectra because they are not infrared active.[22] In the Raman intensity calculations a temperature T of 273 K is used. The polarization vector E is chosen to be (1,1,1). In the figures intensities of lines with a wavenumber difference less than 2 cm^{-1} are added.

Mode Analysis

The results of the rigid ion and shell model calculations are analyzed by using a mode analysis method that allows a prediction of the number of infrared- and Raman-active stretching modes for each irreducible representation of the space group of the structure. Since this method has been discussed extensively elsewhere,[36] it will be briefly summarized here. Based on a calculation within the Bethe lattice approximation one finds that the four Si–O stretching vibrations of the isolated SiO$_4$ tetrahedron transform into two localized and two delocalized stretching vibrations for a structure containing one SiO$_2$ unit per unit cell. Structures containing n SiO$_2$ units per unit cell contain $2n$ localized and $2n$ delocalized Si–O pure stretching vibrations. (In this context the term "vibration" is used for a single eigenvector of the dynamical matrix. So a vibration can be part of a "mode", i.e. a degenerate group of lattice vibrations belonging to the same group theoretical irreducible representation.) In other words, the total number of stretching vibrations is equal to the number of Si–O bonds per unit cell. The localized vibrations can be found in very narrow frequency regions whereas the delocalized vibrations have a broad frequency distribution. Because there have to be $9n - 3$ optical vibrations, $5n - 3$ optical vibrations are bending and torsional vibrations with a wavenumber below approximately 500 cm^{-1}.[36]

By use of SiOSi units instead of SiO$_4$ tetrahedra, one set of n localized and n delocalized modes can be considered to originate from the antisymmetric Si–O–Si stretching vibrations located between 950 and 1200 cm^{-1} as shown in ref 36 for an Si–O–Si angle of 149°. The other set of n localized and delocalized modes can be considered to be derived from the symmetric Si–O–Si stretching vibrations and is located between 450 and 850 cm^{-1}. The localized modes mainly derive from the antisymmetric SiO$_4$ stretching vibrations of F_2 symmetry and are located at the top of the respective frequency regimes, the delocalized modes mainly derive from the symmetric SiO$_4$ stretching vibration of A_1 symmetry with their main spectral weight at the bottom of their frequency regimes.

This result is very similar to that proposed by Galeener[37] for v-SiO$_2$. The extension to n SiO$_2$ units per unit cell can be regarded as the extended Galeener assignment.

The usual factor group analysis of a structure results in the total number of infrared- and Raman-active modes but does not predict the distribution of these modes over stretching, bending, and torsional modes.

The number of stretching vibrations has been determined by a method adapted from the work by Ariai and Smith.[38] The stretching vibrations can be divided into symmetric and antisymmetric vibrations according to their symmetry in a SiO$_4$ tetrahedron. If the SiO$_4$ tetrahedron is part of the zeolite network,

(34) Catlow, C. R. A. *Proc. R. Soc. London* **1977**, *A353*, 533.
(35) Sanders, M. J.; Leslie, M.; Catlow, C. R. A. *J. Chem. Soc., Chem. Commun.* **1984**, 1271–1273.

(36) van Santen, R. A.; Vogel, D. L. *Adv. Solid State Chem.* **1988**, 151.
(37) Galeener, F. L.; Leadbetter, A. J.; Springfellow, M. W. *Phys. Rev. B* **1983**, *27*, 1052.
(38) Ariai, J.; Smith, S. C. P. *J. Phys. C* **1981**, *14*, 1193.

the vibrations of the SiO_4 unit will transform according to specific irreducible representations of the small group of the space group of the crystal. The direct products of the site representations with the irreducible representations of the small group correlating with the F_2 and A_1 species of T_d give the numbers of antisymmetric and symmetric stretching vibrations per symmetry species of the small group. The numbers are obtained by reduction of the direct products into the irreducible representations of the point group. The ratio between the total number of antisymmetric and the total number of symmetric stretching vibrations, so counting m-fold degenerate modes m times, remains equal to that in the free SiO_4 molecule (i.e. three) even if the degeneracy is lifted under a lower symmetry.

The method has been illustrated in detail for ferrierite in ref 36 and will be illustrated for α-quartz in the Appendix. The technique cannot easily be extended to the bending and torsional modes since the number of these modes is not porportional to the number of SiO_2 units per unit cell. Here projection techniques will have to be used to derive the number of modes corresponding to the bending of the SiO_4 tetrahedron.

In the figures showing the results of the calculations, the computed longitudinal (L) and not purely longitudinal (T) frequencies are presented. The longitudinal modes can only be Raman active.

Experimental Section

The infrared spectra of sodalite and faujasite presented here were recorded on a Bruker Model 113-v Fourier transform spectrophotometer. The Raman spectra were obtained from a rotating powder sample with a Jobin Yvon HG2S double monochromator and a Spectra Physics 2020–05 argon ion laser (wavelength of incident radiation 514.5 nm) in zz geometry. The sample of silica–sodalite had been prepared by Keysper.[39] The faujasite sample was dealuminated by flushing a dried sample for 4 h with saturated $SiCl_4$ vapor at 500 °C (a method described by Beyer and Belenykaja[40]) after which treatment the product was flushed with dried N_2 at 500 °C and washed with water at room temperature until no more Cl^- was detected. A commercial NaY zeolite (Ketjen) was used as starting material. Infrared and ^{29}Si NMR spectra indicated that the ratio of framework aluminum ions over silicon ions was less than 0.5%.
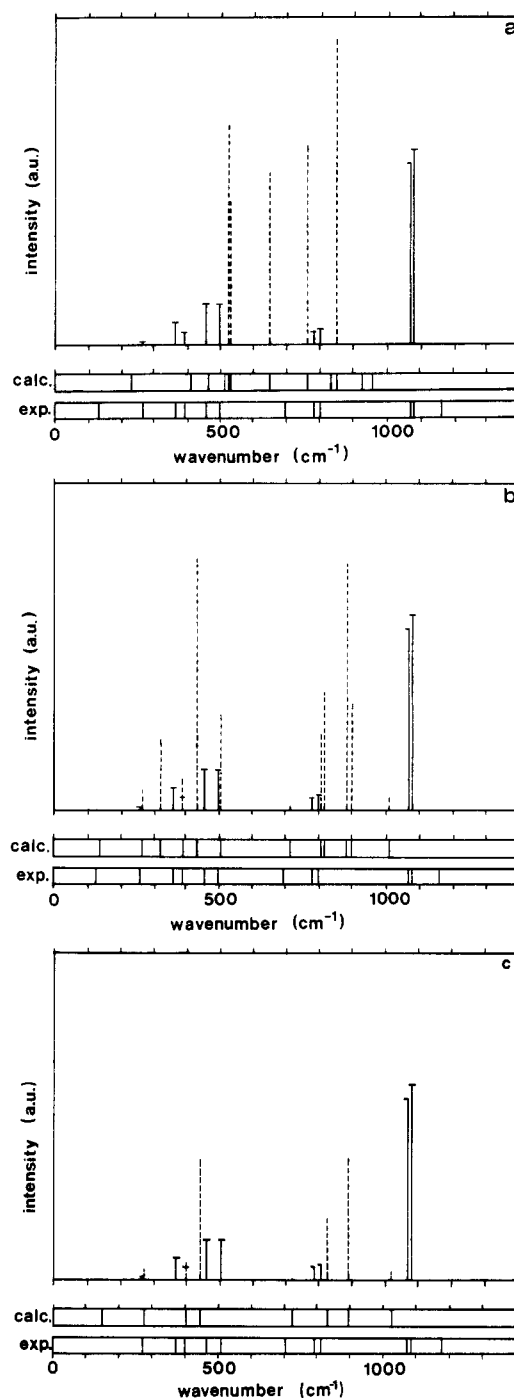
Computed Infrared and Raman Spectra of α-Quartz

As discussed earlier the interatomic potentials used here were derived from the structural and elastic properties of α-quartz. The computed infrared and Raman spectra of α-quartz using these potentials are therefore of interest.

A structure given by Wyckoff[41] with symmetry D_3^4 is used as a starting structure for the relaxation.

Figure 1 shows the calculated and measured[21] infrared spectra of α-quartz; Figure 2 shows the same for the Raman spectra. Calculations are performed for a zero wave vector and for two wave vectors with a length of 0.001 reciprocal lattice unit, one in the direction of the a axis (coinciding with a diad axis) and the other in the direction of the c axis (coinciding with the triad axis). As both the number of infrared modes and the frequencies of these modes are the same for the zero and the $(k,0,0)$ wave vector, the infrared spectrum of the latter is not given. The same applies with respect to the Raman spectrum of the $(0,0,k)$ wave vector.

It is obvious that there are rather large discrepancies between observed and calculated spectra, especially for the rigid ion calculation. The zero wave vector shell model calculations (Figures 1b and 2b) represent the low frequencies better than the rigid ion calculations but differences remain in the high-frequency region.

The frequencies of the normal modes are given in Figure 3. For nonzero wave vectors k, the names of the irreducible repre-

(39) Keysper, J., private communication.
(40) Beyer, H. K. I.; Belenykaja, I. *Catalysis by Zeolites*; Imelik, B., Ed.; Elsevier: Amsterdam, 1980; p 203.
(41) Wyckoff, R. W. G. *Crystal Structures*; Wiley: New York, 1964; Vol. 1.

Figure 1. Infrared spectra of α-quartz: (a) rigid ion model $k = 0$; (b) shell model $k = 0$; (c) shell model $k = (0,0,0.001)$; solid lines with bar, experimental;[21] broken lines, calculated.
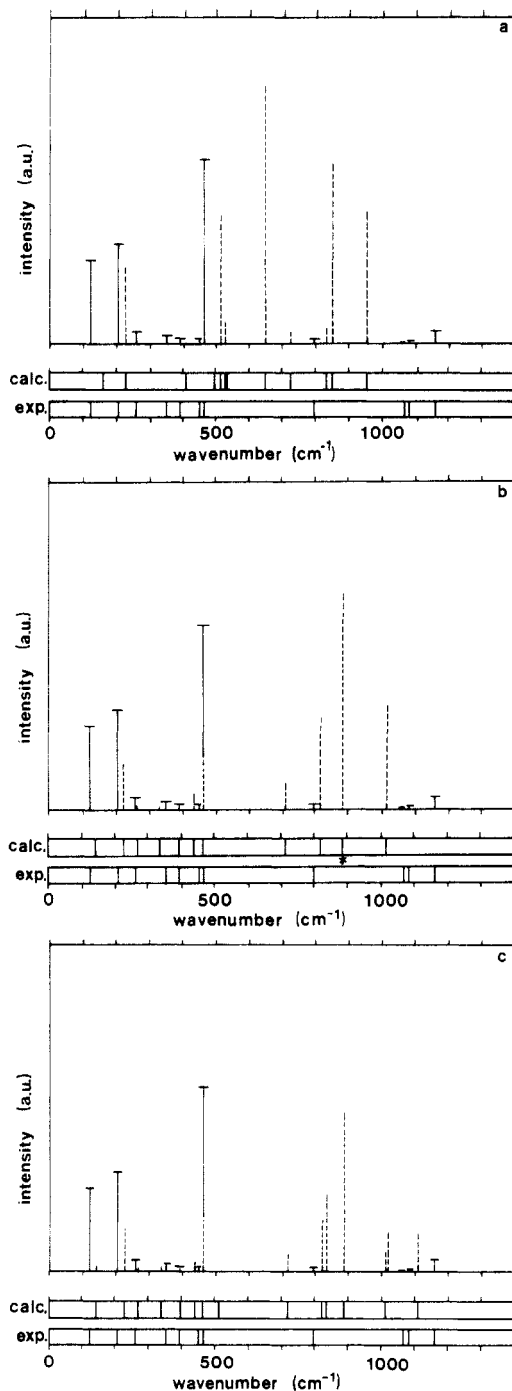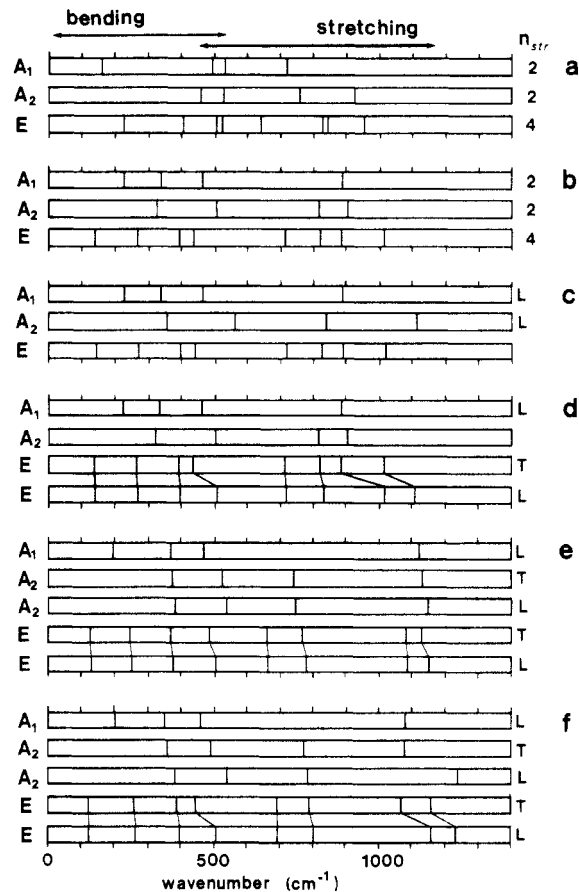
sentations for a zero wave vector are used (compare ref 22) because the wave vectors used are so small. To show the effect of T–L splitting a distinction is made between purely longitudinal (labeled L) modes and not purely longitudinal (labeled T) modes. The A_1 modes, that are longitudinal for the wave vectors used, have no polarization associated with them in the limit $k \to 0$[22] so they are not called longitudinal in Figure 3.

One predicts (for a zero wave vector) with the group theoretical method discussed earlier,[36] based on the Bethe lattice approximation combined with a group theoretical analysis, the number of infrared-active stretching modes (having a wavenumber larger than about 450 cm^{-1}) to be six and the number of Raman-active stretching modes to be six too. The total number of stretching vibrations adds up to 12, because of the 2-fold degeneracy of the E modes, and is of course equal to the sum of the numbers of symmetric ($2n$) and antisymmetric stretching vibrations ($2n$), n being equal to three. When we compare this with the compu-

Figure 2. Raman spectra of α-quartz: (a) rigid ion model $k = 0$; (b) shell model $k = 0$; (c) shell model $k = (0,0,0.001)$; solid lines with bar, experimental;[21] broken lines, calculated.

Figure 3. Normal mode analysis of α-quartz: (a) rigid ion model $k = 0$; (b) shell model $k = 0$; (c) shell model $k = (0,0,0.001)$; (d) shell model $k = (0.001,0,0)$; (e) calculated by Striefler and Barsch;[24] (f) experimental modes[20,61] except for the two lowest longitudinal E modes which are calculated by Elcombe[22] from the corresponding transversal mode frequencies, the high-frequency dielectric constants and the static dielectric constants. n_{str} equals the number of stretching modes as expected from the Bethe lattice approximation. L, longitudinal mode; T: not pure longitudinal mode.

tational and the experimental results, we see that one A_1 mode is found in the frequency region where both stretching and bending modes exist (Figure 3). Clearly, the rigid ion model results do not simulate the experimental data very well because of the dominance of the long range electrostatic interactions in this model. Since the long-range electrostatic interactions are screened in the shell model calculations due to the polarization of the oxygen ions, the short range potentials are much improved. This is reflected in the reasonably good agreement found for the bending as well as the torsional modes.

The shell model calculations reproduce the "quartz frequency gap" between 500 and 700 cm^{-1}[36] rather well. Also the division of the Si–O stretching modes into symmetrical Si–O–Si modes in the frequency regime around 700 cm^{-1} and antisymmetrical Si–O–Si modes at higher frequencies is nicely reproduced. However, the average position as well as the frequency difference between the symmetrical and antisymmetrical regimes is too small.

The calculated line intensities for the rigid ion spectra are in poor agreement with experiment. The shell model gives reasonably good infrared intensities but the Raman intensities are poor.

One concludes that the attractive component of the Si–O (two-body) potential is too small, resulting in values of the Si–O stretch frequencies being too low. This follows because the average position as well as the frequency difference between the symmetrical and antisymmetrical modes in the stretching regime are proportional to the Si–O stretch frequency of a free Si–O oscillator.[36] Whether the poor results for the line intensities have to be contributed to poor atomic displacement vectors or to a poor approximation in formulas 5 and 8 cannot be judged from these results.

Computed Infrared and Raman Spectra of Silica–Sodalite

The structure of aluminum–sodalite belongs to space group $P\bar{4}3n$ or T_d^4.[42] A small shift in the position of oxygen in aluminum-free sodalite (from $x/a = 0.150$, $y/b = 0.135$, $z/c = 0.440$ to $x/a = y/b = 0.142$, $z/c = 0.440$) results in a change from space group T_d^4 to T_d^3 or $I\bar{4}3m$.[36]

The nonzero wave vectors chosen are pointed along a triad axis (a body diagonal of the unit cell) and along a diad axis (in our case the c axis). In Figure 4 only infrared spectra for the zero wave vectors are given, because the frequencies of the infrared-active lines are the same for nonzero and zero wave vectors. Of course the line intensities differ for different wave vectors. In

(42) This is the commonly used space group. $P\bar{4}3m$ and $I\bar{4}3m$ have been used too. For a discussion see: Wyckoff, R. W. G. *Crystal Structures*, 2nd ed.; Wiley: New York, 1968.
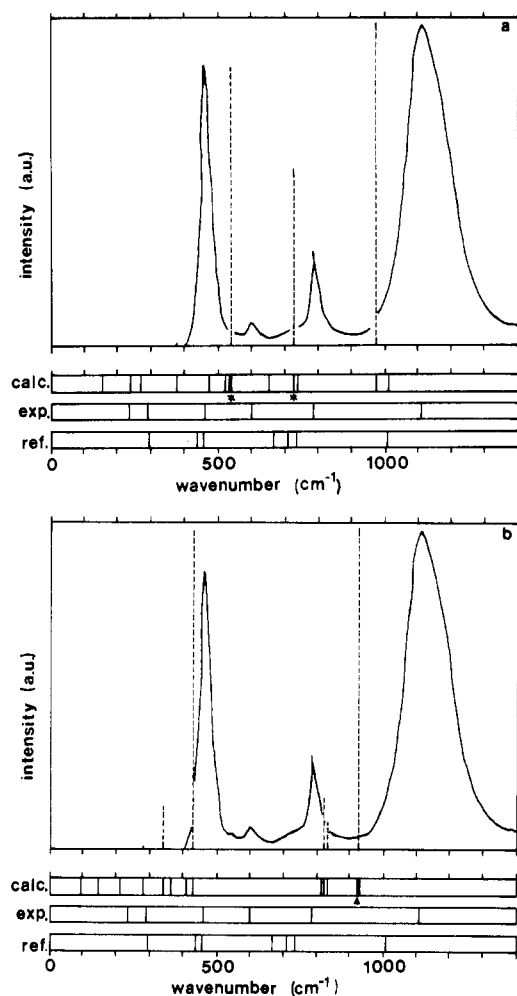
Figure 4. Infrared spectra of silica–sodalite (T_d^4): (a) rigid ion model $k = 0$; (b) shell model $k = 0$; solid line, experimental; broken lines, calculated. The reference values are from Godber and Ozin[45] for a high-silica sodalite (Si/Al = 1.93). Asterisk indicates two active modes. Triangle indicates three active modes.

Figure 5 the spectrum for the wave vector (0,0,0.001) is not given because the calculated frequencies turn out to be almost equal to those of the (0.001,0.001,0.001) wave vector. Again, the intensities are different but show the same trend. The calculated intensities agree slightly better with experiment than those of α-quartz.

The number of infrared-active stretching modes (>600 cm^{-1}) observed experimentally (Figure 4) for high-silica sodalite agrees well with the number predicted for the T_d^3 structure (three modes vs. six for T_d^4 sodalite).[36] However, the line at highest frequency (1107 cm^{-1}) might be composed of several components so a slight deviation from the given symmetry is possible. This deviation would agree with Meinhold and Bibby's[43] observation of the presence of nonequivalent silicon sites in sodalite. The predicted number of Raman-active stretching modes is six for the structure with T_d^3 symmetry and 12 for the T_d^4 structure. This appears to agree with the experimental Raman spectrum (Figure 5) if comparison is made with the Raman spectrum predicted according to the rigid ion model. Angell[44] has measured a Raman spectrum of natural sodalite with lines at 260, 290, 463, 985, and 1060 cm^{-1}. These frequencies are reproduced very well by the shell model calculation. The better agreement of this calculation with natural sodalite is understandable since in natural sodalite the silicon-aluminum ratio is about one. As a result, the average stretching force constant is weaker than in aluminum-free sodalite and the results of the shell model calculations on α-quartz already indicated that the Si–O bonding in the potential used is too weak.
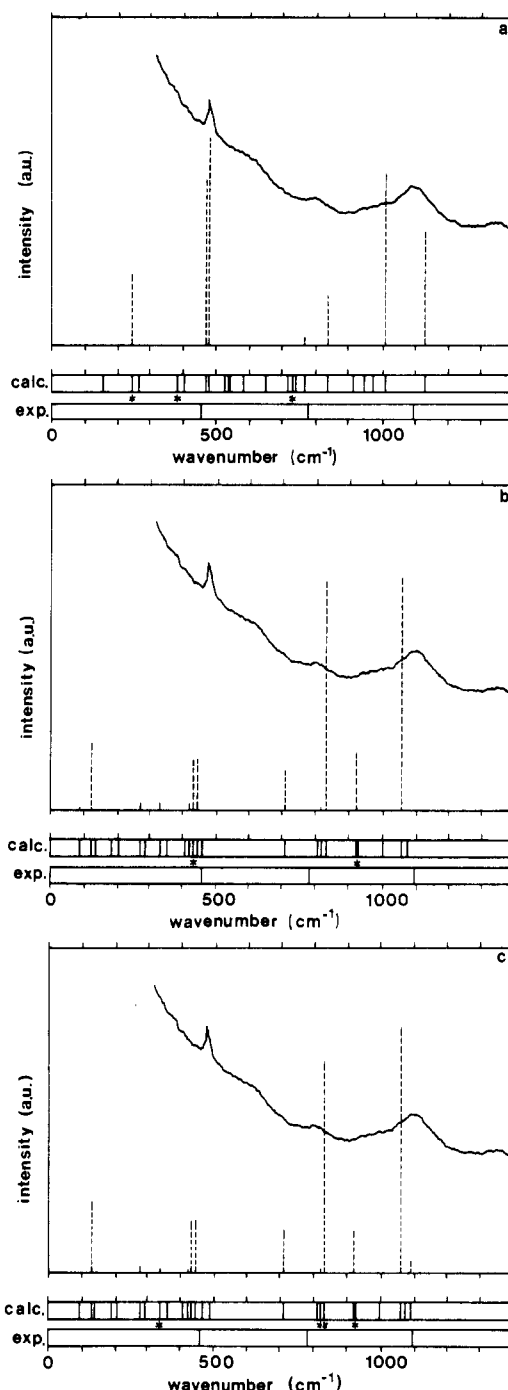
Figure 5. Raman spectra of silica–sodalite (T_d^4): (a) rigid ion model $k = 0$; (b) shell model $k = 0$; (c) shell model $k = (0.001,0.001,0.001)$; solid line, experimental; broken lines, calculated. Asterisk indicates two active modes. Triangle indicates three active modes.

For the shell model calculation on this zeolite, as in the case of α-quartz, we observe a frequency region of both stretching and bending modes (Figure 6). The calculated spectra shown in Figures 4, 5, and 6 are made by using the relaxed T_d^4 structure with the initial structure taken from Wyckoff.[41]

The spectrum of high-silica sodalite has recently become available in the far-infrared region from the work of Godber and Ozin.[45] Their observation of an infrared-active framework bending mode at 289 and 231 cm^{-1} agrees well with our calculated value. The absorption band around 500 cm^{-1}, due to an O–Si–O bending mode, is reasonably well reproduced in the rigid ion model as well as the shell model calculations. The three predicted Si–O stretching modes are well reproduced in the shell model calcu-

(43) Meinhold, R. H.; Bibby, D. M. *Zeolites* **1986**, *6*, 427.
(44) Angell, C. L. *J. Phys. Chem.* **1973**, *77*, 222.

(45) Godber, J.; Ozin, G. A. *J. Phys. Chem.* **1988**, *92*, 2841.
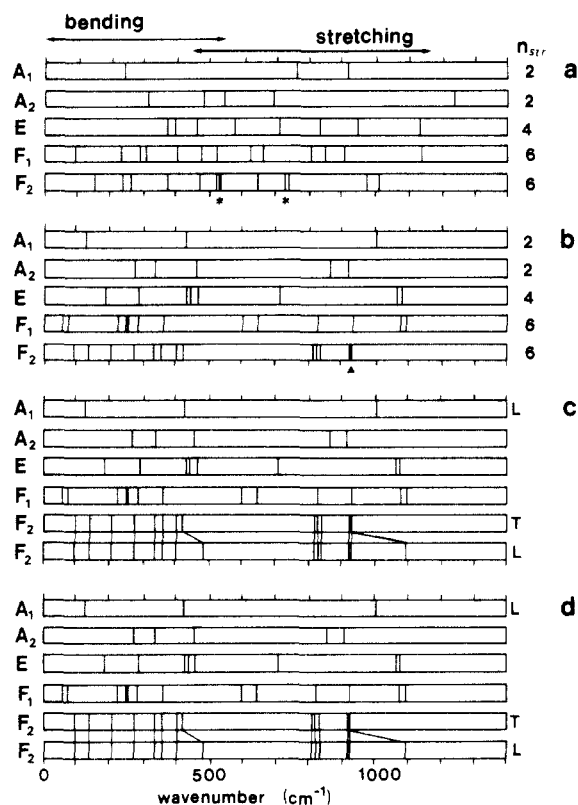
Figure 6. Normal mode analysis of silica–sodalite (T_d^4): (a) rigid ion model k = 0; (b) shell model k = 0; (c) shell model k = (0.001,0.001,0.001); (d) shell model k = (0,0,0.001). n_{str} equals the number of stretching modes as expected from the Bethe lattice approximation. L is longitudinal mode; T is not pure longitudinal mode. Asterisk indicates two active modes. Triangle indicates three active modes.

lations. Again the effect is observed of the calculated Si–O bond stretch frequencies being too low. The peak at 600 cm⁻¹ has to be assigned to carbonaceous residue left in the material after calcination of the synthesized sample.
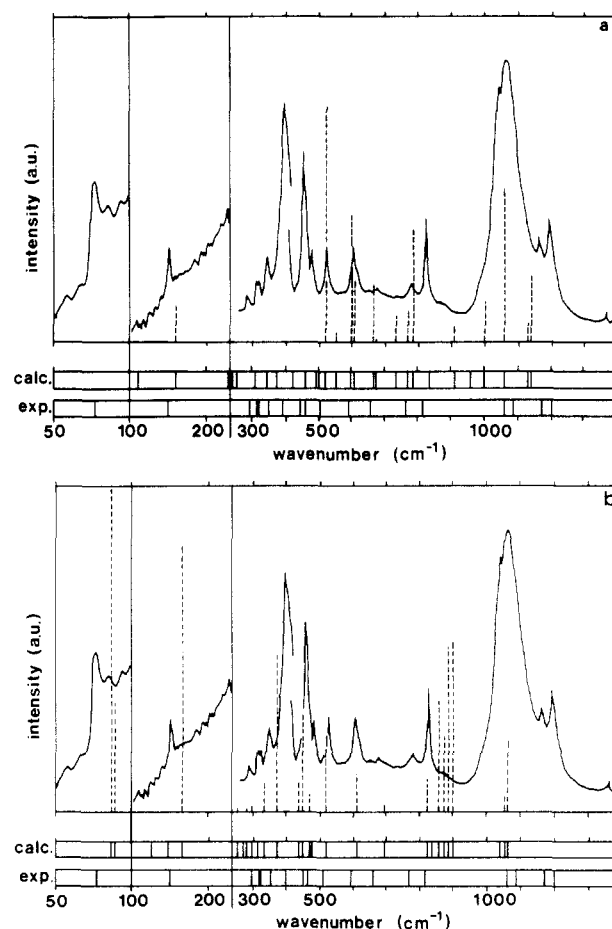
Computed Infrared and Raman Spectra of Faujasite

Figures 7, 8, and 9 show the experimental and calculated spectra for faujasite (space group $Fd3m$ or O_h^7). The nonzero wave vectors chosen are pointed along a 4-fold axis (in this case the c axis) and along a triad axis (a body diagonal).

In Figure 7 only the infrared spectra for the zero wave vectors are given, because the frequencies of the infrared-active lines are the same for nonzero and zero wave vectors. Of course the line intensities differ for different wave vectors. The agreement of calculated intensities with experiment is not too bad in both the rigid ion calculation and the shell model calculation.

The data for the initial structure were obtained from Hseu.[46]

The number of infrared-active modes predicted in the Si–O stretching regime for faujasite equals 12. This agrees well with the total number observed in the stretching regime.

The predicted number of Raman-active stretching modes is 24 but this number cannot be verified from the experimental spectrum. Because of the huge amount of infrared lines, both calculated and observed, a sharp distinction between the quality of the rigid ion and the shell model cannot be made. It is noteworthy that also according to the Shell model calculations, infrared-active modes appear in the "quartz frequency gap" (between 500 and 700 cm⁻¹). This is in agreement with the experiments. Again the calculated Si–O stretch frequencies appear to be underestimated. The experimental infrared data of dealuminated faujasite have been published earlier in paper 36. The peaks at 77 and 150 cm⁻¹ clearly originate from incompletely removed sodium.[47,48] The

(46) Hseu, T. Ph.D. Thesis, University of Washington, University Microfilms 73-13835 Ann Arbor, MI, 1973.
(47) Miecznikowski, A.; Hanuza. J. *Zeolites* **1985**, *5*, 188.

Figure 7. Infrared spectra of dealuminated faujasite: (a) rigid ion model k = 0; (b) shell model k = 0; solid line, experimental; broken lines, calculated; (*) two active modes; (△) three active modes. The full scale intensities in the right part of the figures (230–1400 cm⁻¹) are 20 times larger than those in the middle part (100–230 cm⁻¹) and left part (50–100 cm⁻¹).

TABLE IV: Observables of α-Quartz

observable	experimental	rigid ion	shell model	unit
c_{11}	8.683[b]	20.2343	9.4458	10^{11} dyn/cm²
c_{33}	10.60[b]	21.2907	11.6075	10^{11} dyn/cm²
c_{44}	5.826[b]	6.3078	5.0083	10^{11} dyn/cm²
c_{66}	3.987[b]	6.7995	3.8203	10^{11} dyn/cm²
c_{12}	0.71[b]	6.6353	1.8369	10^{11} dyn/cm²
c_{13}	1.193[b]	8.6264	1.9675	10^{11} dyn/cm²
c_{14}	−1.806[b]	0.0	−1.4525	10^{11} dyn/cm²
ϵ_{xx}^0	4.520[c]	3.8999	4.7394	
ϵ_{zz}^0	4.640[c]	4.0689	5.0135	
ϵ_{xx}^∞	2.356[d]	a	2.1162	
ϵ_{zz}^∞	2.356[d]	a	2.1394	
E	−13421[e]	−11956	−12417	kJ/mol of SiO_2

^{a} The rigid ion model does not give a high frequency dielectric constant. ^{b} Reference 59. ^{c} Reference 14. ^{d} Reference 60. ^{e} Reference 50.

low-frequency bending modes in the infrared spectrum also agree well with the data from Godber and Ozin.[45] They observed a triplet of low intensity between 250 and 350 cm⁻¹ that is also reproduced in the calculation.
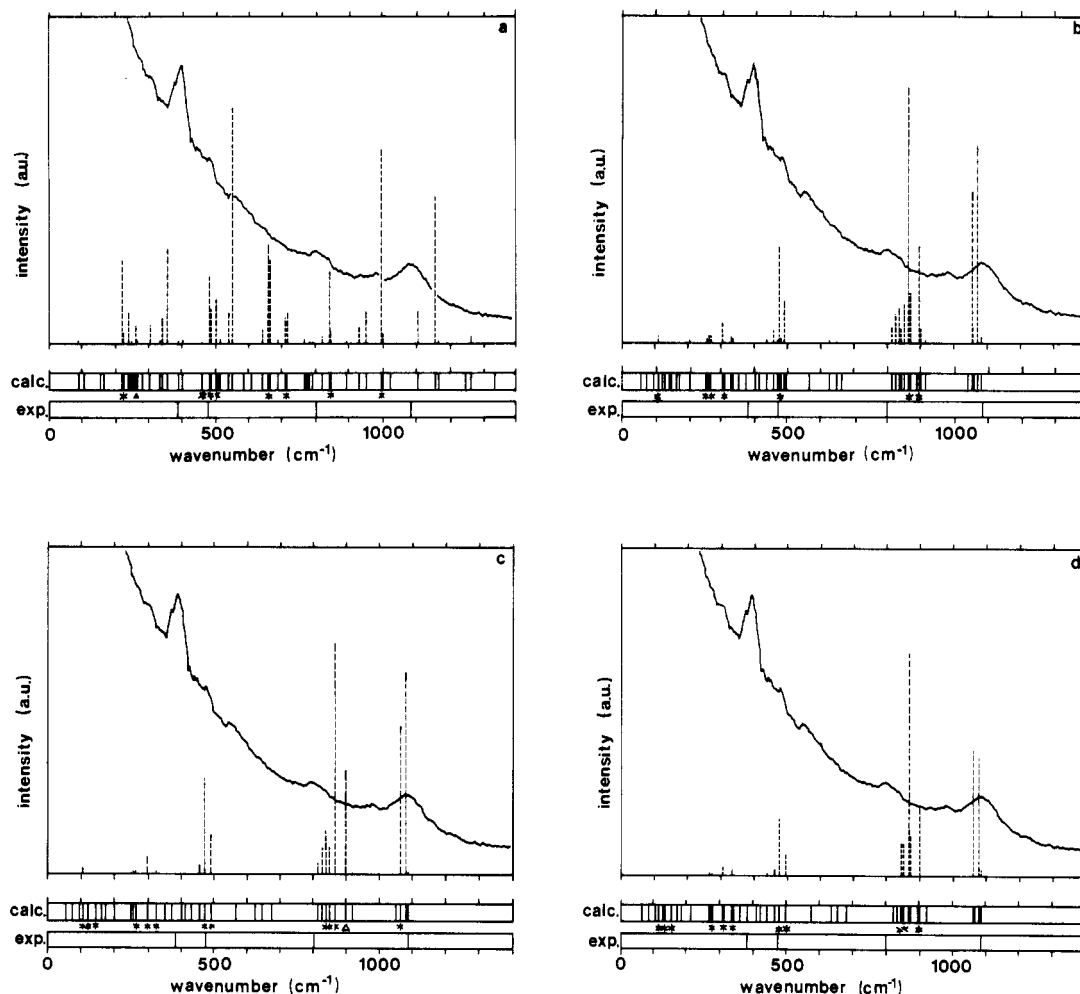
Comparison with Other Observables

The quality of the model can also be checked by comparing observed and calculated values of the independent elastic constants c_{11}, c_{33}, c_{44}, c_{66}, c_{12}, c_{13}, and c_{14}, the static dielectric constants ϵ_{ij}^0, the high frequency dielectric constants ϵ_{ij}^∞, and the lattice energy E.

(48) Peuker, C. H.; Moeller, K.; Kunath, D. *J. Mol. Struct.* **1984**, *114*, 215.

Figure 8. Raman spectra of dealuminated faujasite: (a) rigid ion model $k = 0$; (b) shell model $k = 0$; (c) shell model $k = (0.001,0.001,0.001)$; (d) shell model $k = (0,0,0.001)$; solid line, experimental; broken lines, calculated; (*) two active modes; ($\triangle$) three active modes.

For zeolites information on these parameters is lacking but for α-quartz values are well-known[23,24] (Table IV). The sign of the c_{14} constant is in accordance with the convention discussed by Barron et al.[23] The rigid ion model does not give a value of the high-frequency dielectric constant.

We observe a large difference between the observed values and those calculated with the parameters optimized to fit the structure according to the rigid ion model. The differences occur as a result of the energy minimization. Agreement with observables calculated with the shell model is much better.

From Hückel calculations[8] a value of $-13\,202$ kJ/mol of SiO_2 for the lattice energy of α-quartz can be derived. A similar calculation results in a lattice energy of aluminum-free faujasite of $-13\,211$ kJ/mol of SiO_2.

Experimental values of the lattice energy of α-quartz are $-13\,421$ kJ/mol of SiO_2[49] and $-13\,134$ kJ/mol of SiO_2.[50] Reference values for the ionic polarizability of O^{2-} ions in a SiO_2 crystal are 1.7 Å³ [51] and 1.984 Å³.[52] The value for the free ion given by the parameters of the Shell model is 1.582 Å³ and the value for the ion in the lattice is 1.354 Å³.[3] The ionic polarizability of Si^{4+} is much smaller[52] than the O^{2-} value, viz. 0.0256 Å³, and is ignored in the shell model calculation.

From measurements made by Schoonheydt[53] one can estimate a value of the static dielectric constant ϵ^0 of NaY-zeolite between

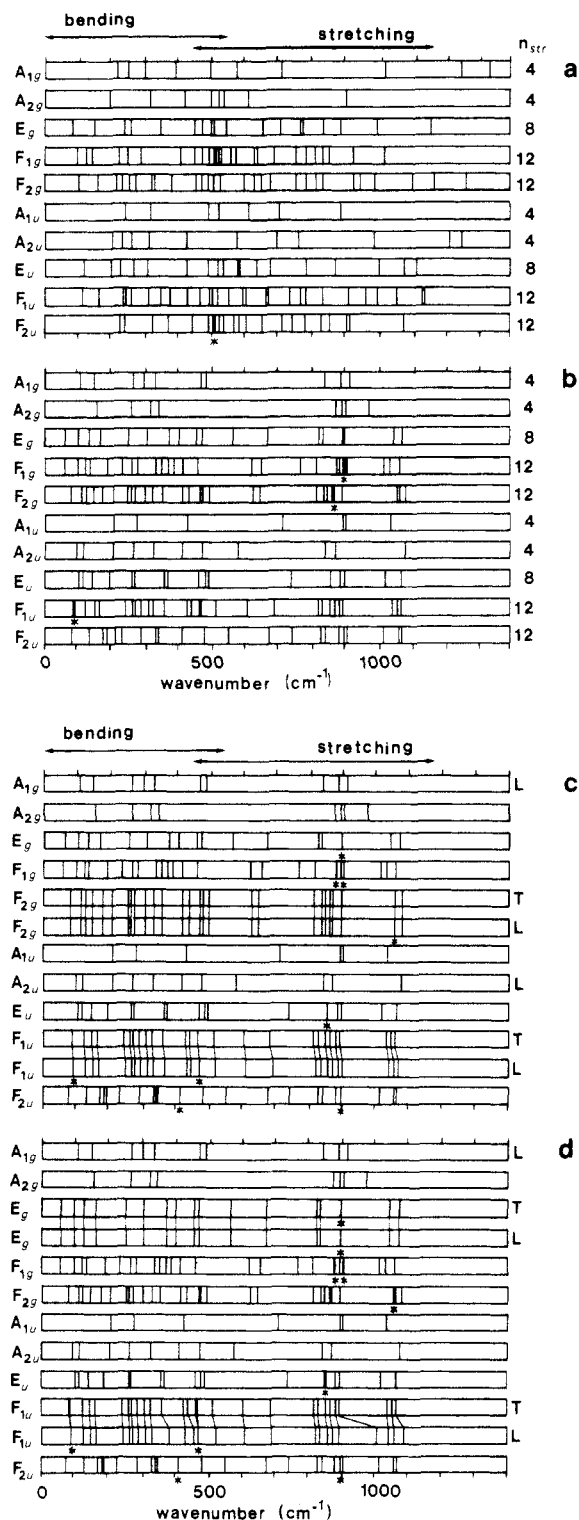(49) Robie, R. A. *U.S. Geol. Surv. Bull.* **1978**, *No. 1452.*

(50) Samsonov, G. V. *The Oxide Handbook*; IFI/Plenum: New York, 1973.

(51) Tessman, J. R.; Kahn, A. H. *Phys. Rev.* **1953**, *92*, 890.

(52) Greenwood, N. N. *Ionen, Kristalle, Gitterdefekte und Nichtstoichiometrische Verbindungen*; Verlag Chemie: Weinheim, 1973.

(53) Schoonheydt, R. A. In *Proceedings of the International Conference on Zeolites, 5th*, Naples; Rees, L. V., Ed.; Heyden: London 1980.

TABLE V: Calculated Observables for Zeolitic Polymorphs

observable	sodalite[a] rigid	sodalite[a] shell	sodalite[b] rigid	sodalite[b] shell	faujasite rigid	faujasite shell	unit
c_{11}	14.74	8.51	14.38[c]	8.32[c]	8.21	8.43	10^{11} dyn/cm²
c_{44}	3.81	2.30	3.63[c]	2.22[c]	2.66	5.16	10^{11} dyn/cm²
c_{12}	5.54	1.81	5.70[c]	1.90[c]	4.08	2.08	10^{11} dyn/cm²
ϵ_{xx}^0	2.83	3.32	2.87[c]	3.36[c]	2.31	2.64	
ϵ_{xx}^∞	d	1.70	d	1.70[c]	d	1.50	
ΔE^e	1	13	0.2	12.6	44	19.5	kJ/mol of SiO_2

[a] Sodalite structure restricted to symmetry T_d^4. [b] Sodalite structure restricted to symmetry T_d^3. [c] The relaxed structure is not cubic. Mean values of constants are given. [d] The rigid ion model does not give a high-frequency dielectric constant. [e] $\Delta E = E_{zeolite} - E_{quartz}$: for the rigid ion model, $E_{quartz} = -11956$ kJ/mol of SiO_2; for the shell model, $E_{quartz} = -12417$ kJ/mol of SiO_2.

3.4 and 4.7. Note that the simulations are performed for aluminum-free (and sodium-free) zeolites.

Table V gives the values of the observables for the calculated aluminum-free zeolites. The differences between the results for sodalite with the T_d^4 and T_d^3 structure are not large although the relaxed structures are different. One observes from the computed energies of the sodalitic and faujasitic polymorphs that the energy differences between sodalite and α-quartz increase and the energy difference between faujasite and α-quartz significantly decrease, if rigid ion results are compared with the results of shell model calculations.

Faujasite is the material of lowest density. The energy difference between this material and α-quartz is, according to the rigid ion model, 44 kJ/mol of SiO_2. The smaller value found according to the shell model calculation suggests that energy differences computed according to the rigid ion model are probably

Figure 10. $\epsilon_{\alpha\alpha}^{0}/\epsilon_{\alpha\alpha}^{\infty} - 1$ versus density for α-quartz, sodalite, and faujasite: +, calculated by THBREL; $\times$, calculated from optical frequencies (formula 9); $\bullet$, experimental data.[14,60] For α-quartz values of $\epsilon_{xx}^{0}/\epsilon_{xx}^{\infty} - 1$ (labeled with x) and $\epsilon_{zz}^{0}/\epsilon_{zz}^{\infty} - 1$ (labeled with z) are given.

TABLE VI: Derivatives of Two-Body Potentials

			Si–O ($r = 1.61$ Å)		O–O ($r = 2.60$ Å)	
potential[a]	ref	Si charge, e	$dV/r\,dr$, eV/Å²	d^2V/dr^2, eV/Å²	$dV/r\,dr$, eV/Å²	d^2V/dr^2, eV/Å²
rigid ion	h.l.	4.0	12.02	6.10	−3.20	6.02
shell model	h.l.	4.0	12.65	17.16	−4.70	8.87
rigid ion, NNB	22	1.94	5.63	27.51	−1.51	2.46
BVK, NNB	22	0.0	3.37	27.06	−0.78	3.05
rigid ion, NNB	23	1.94	5.53	27.03	−1.51	2.44
BVK, NNB	23	0.0	3.28	26.32	−0.78	3.05
BLSF	16	0.0		21.791		
BLSF²	16	0.0		21.891		
BLSF-BR	16	0.0		31.735		
GVFF	17	0.0		20.16		
GVFF	20	0.0		26.96		
GVFF	21	0.0		37.09		
GVFF	37	0.0		29.87		

[a] Key: NNB, short range interactions only for nearest neighbors; BVK, Born–von Kármán model (zero charges); GVFF, generalized valence force field; BLSF, $d^2V/dr^2 = k'(r'/r)^{3/2}$; BLSF2, $d^2V/dr^2 = k'(r'/r)^3$ with $k' = 21.693$ eV/Å² and $r' = 1.6149$ Å; BLSF-BR, $d^2V/dr^2 = c(r - b)^{-3}$ with $c = 9.545$ eV Å and $b = 0.94$ Å.

using data from α-quartz, sodalite, and faujasite. The ratio $\epsilon_{\alpha\alpha}^{0}/\epsilon_{\alpha\alpha}^{\infty}$ can be calculated directly by the energy minimization program (Table V) but also from the difference between longitudinal and transversal frequencies using the well-known Lyddane–Sachs–Teller relation expressed in formula 9

$$\frac{\epsilon_{\alpha\alpha}^{0}}{\epsilon_{\alpha\alpha}^{\infty}} = \frac{\prod(\omega_{L\alpha})^2}{\prod(\omega_{T\alpha})^2} \tag{9}$$

where α is the Cartesian component, $\omega_{L\alpha}$ is the frequency of longitudinal vibration with polarization in direction α, and $\omega_{T\alpha}$ is the frequency of transversal vibration with polarization in direction α. The product is taken over all optical modes.

Values of the ratio calculated in this way are also included in Figure 10. A very satisfactory agreement between the values of the ratio $\epsilon_{\alpha\alpha}^{0}/\epsilon_{\alpha\alpha}^{\infty}$ calculated in these two ways is found. The rather high theoretical values of $\epsilon_{\alpha\alpha}^{0}/\epsilon_{\alpha\alpha}^{\infty}$ compared with experimental values of α-quartz again indicate the overestimation of the electrostatic effects.

Discussion and Conclusions

For a comparison with other model calculations the first and second derivatives of the two-body potentials are given in Table VI. The derivatives are calculated for a Si–O distance of 1.61 Å and a O–O distance of 2.60 Å. The first derivative is divided by the distance. The nearest neighbor Coulomb interaction is included. For the shell model only the O^{shell}–Si^{core} interaction is calculated. We see that the potentials employed in this study have smaller first and second derivatives of the potential than those
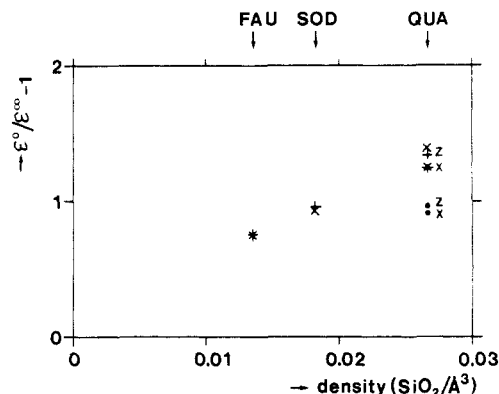

Figure 9. Normal mode analysis of dealuminated faujasite: (a) rigid ion model $k = 0$; (b) shell model $k = 0$; (c) shell model $k = (0.001,0.001,0.001)$; (d) shell model $k = (0,0,0.001)$. n_{str} equals the number of stretching modes as expected from the Bethe lattice approximation; L, longitudinal mode; T, not pure longitudinal mode; and *, two active modes.

overestimated (compare the energy difference between faujasite and sodalite) because the long range electrostatic potential is not screened in the rigid ion model.

For a cubic diatomic crystal the value of $\epsilon_{xx}^{0}/\epsilon_{xx}^{\infty} - 1$ should decrease with increasing density, since it is proportional to the plasma frequency.[54] This relation is expressed in Figure 10 by

(54) Bilz, H.; Strauch, P.; Wehner, R. K. *Handbuch der Physik Band XXV/2d Licht und Materien*, Springer, Verlag: Berlin 1984; p 69.

TABLE VII: Character Table of D_3, $\Gamma_{3a}{}^s$, $\Gamma_{3a}{}^s \cdot A_1$, $\Gamma_{3a}{}^s \cdot A_2$, and $\Gamma_{3a}{}^s \cdot E$

D_3	E	$2C_3(z)$	$3C_2'$	
A_1	1	1	1	Raman active
A_2	1	1	-1	infrared active
E	2	-1	1	Raman, infrared active
$\Gamma_{3a}{}^s$	3	0	1	
$\Gamma_{3a}{}^s \cdot A_1$	3	0	1	decomposition: $A_1 + E$
$\Gamma_{3a}{}^s \cdot A_2$	3	0	-1	decomposition: $A_2 + E$
$\Gamma_{3a}{}^s \cdot E$	6	0	0	decomposition: $A_1 + A_2 + 2E$

TABLE VIII: Correlation Table for T_d and D_3 (via O)^a

T_d	O	D_3
A_1	A_1	$\underline{A_1}$
	A_2	A_2
F_2	F_1	$\underline{A_2} + \underline{E}$
	F_2	$A_1 + E$

^{a} Irreducible representations of D_3 that correlate with those of T_d are underlined.

TABLE IX: Number of Stretching Vibrations and Modes

	no. stretching vibrations^a	no. stretching modes^a
A_1	$1(A_1) + 1(F_2) = 2$	$1(A_1) + 1(F_2) = 2$
A_2	$2(F_2) = 2$	$2(F_2) = 2$
E	$2(A_1) + 6(F_2) = 8$	$1(A_1) + 3(F_2) = 4$
infrared active	$2(A_1) + 8(F_2) = 10$	$1(A_1) + 5(F_2) = 6$
Raman active	$3(A_1) + 7(F_2) = 10$	$2(A_1) + 4(F_2) = 6$
total	$3(A_1) + 9(F_2) = 12$	$2(A_1) + 6(F_2) = 8$

^{a} The name between parentheses indicates the direct product involved: (A_1), originating from A_1 of T_d; (F_2), originating from F_2 of T_d.

in other studies which use potentials that are fitted on infrared, Raman, and inelastic neutron scattering spectra and as a result show better high frequencies. Determination of the effective second derivative of the Si–O nearest neighbor potential by a numerical analysis of the experimental frequencies in the stretching regime using the first shell Bethe lattice approximation[36] on α-quartz results in a value of the second derivative of 35.19 eV/Å^2.

It should be mentioned that the other models only have short range interactions for nearest (or next-nearest) neighbors. For the bending force constant, reference values are found ranging from 1.052 eV/rad$^{2\ 24}$ to 6.6178 eV/rad^{2,55} The results summarized in Table VI confirm the conclusion of our work that the short range potentials need improvement and that with our potentials the stretch frequencies are underestimated. Probably the most severe assumption made is the use of full formal charges on the cations that result in imprecise short range potentials obtained from the fitting procedure.

The calculation of the line intensities does not indicate that the values of the atomic displacement vectors are completely wrong but the approach to calculate these intensities has to be improved.

Table IV indicates the rather good agreement between experimental elastic constants and calculated values with the shell model parameters used in our studies. This agreement is much better than for the results of rigid ion nearest neighbor and Born–von Kármán model calculations published by others.[22-24] Whereas this suggests that the polarizability that is contained in the shell model calculations is an essential feature of correct potential models, it is more likely than the differences are due to the absence of three-body bending potentials in the work we are making a comparison with.[22-24] This agrees with the rather good correspondence between calculated optical mode frequencies between 100 and 200 cm^{-1} and experimental values. Nonetheless the improvement we find using the shell model indicates that with

the fitting procedure used much better short range potentials have been found, because of the decreased importance of long range electrostatic effects due to screening of the charges.

The results presented also illustrate the power of the group theoretical approach[36] that is not based on model assumptions of the zeolite as required by other approaches.[47] Whereas the infrared spectra appear to contain all theoretically predicted lines, this is not the case for the experimental Raman data because of the low Raman intensities.

Appendix

The method developed in ref 36 to determine the number of stretching vibrations is used here to estimate this number for α-quartz. In this approach the crystal is regarded as being built from tetrahedral SiO$_4$ units.

In a free SiO$_4$ unit of T_d symmetry the symmetrical stretching vibrations transform according to the irreducible representation A_1 and the triply degenerate antisymmetric stretching vibrations transform according to F_2. In the crystal these vibrations will transform according to specific irreducible representations of the small group of the crystal space group. These irreducible representations can generally be found by using correlation tables as given in e.g. ref 56 and 57. To estimate the number of stretching modes, the direct product of these irreducible representations with the site representations of the Si atoms is calculated. This product is decomposed in irreducible representations of the small group.

The space group of α-quartz is $D_3{}^4$ so the small group is D_3. The character table of D_3 is given in Table VII.

In Table VIII the correlation between the irreducible representations of T_d and the irreducible representations of D_3 is shown. Since D_3 is not a subgroup of T_d correlations can only be made by using a point group of higher symmetry (in this case O). As a result irreducible representations in T_d correlate with several irreducible representations of D_3. In order to proceed a choice has to be made. Sometimes this can be done by inspection, for instance when a separation between Raman and infrared active modes can be made, as in the case of ferrierite.[36] In other cases, as in α-quartz, only a full projection operator analysis provides the solution. One finds[58] in the case of α-quartz that the irreducible representations of D_3 that are underlined in Table VIII correlate with the irreducible representations of T_d.

If we regard the Wyckoff sites to be occupied by a set of equivalent atoms, then the site representation has for its characters the number of those atoms which are mapped onto themselves by the symmetry operations of the space group. In α-quartz the three Si atoms are on the 3a site, so on the 2-fold screw axes C_2'. The characters of the site representation $\Gamma_{3a}{}^s$ are given in Table VII, as well as the direct products $\Gamma_{3a}{}^s \cdot A_1$, $\Gamma_{3a}{}^s \cdot A_2$, and $\Gamma_{3a}{}^s \cdot E$ and their decomposition.

In the end the number of stretching modes for every irreducible representation of the small group can be counted. The total

(55) Lazarev, A. N. *Vibrational Spectra and Structure of Silicates*; Consultants Bureau: New York, 1972.

(56) Ferraro, J. R.; Ziomek, J. S. *Introductory Group Theory*; Plenum Press: New York, 1975; p 235.

(57) Salthouse, J. A.; Ware, M. J. *Point Group Character Tables and Related Data*; Cambridge University Press: Cambridge, 1972; p 58.

(58) Vogel, D. L., unpublished results.

(59) Koga, I.; Aruga, M.; Yoshinaka, Y. *Phys. Rev.* **1958**, *109*, 1467.

(60) Spitzer, W. G.; Kleinman, D. A. *Phys. Rev.* **1961**, *121*, 1324.

(61) Krishnamurti, *Proc. Indian Acad. Sci. A* **1958**, *47*, 276.

number of stretching vibrations has to be $4n$ (where n is the number of SiO_2 units in the crystallographic unit cell) so in the case of α-quartz 12 stretching vibrations have to be found.

Table IX gives the number of stretching modes.

The low-frequency stretching modes can be in the same fre-quency region as some bending modes, so one should be careful when counting the number of stretching modes in a spectrum.

Effects of Alkyl Chain Length on the Adsorption of an N-Alkylated Acridine Orange Cation by Colloidally Dispersed Zirconium Phosphate

Masahiro Taniguchi, Akihiko Yamagishi,* and Toschitake Iwamoto

Department of Chemistry, College of Arts and Sciences, The University of Tokyo, 3-8-1 Komaba, Meguro-ku, Tokyo 153, Japan (Received: January 17, 1989; In Final Form: October 13, 1989)

The adsorption of N-alkylated acridine orange derivatives ($AO-C_n$; $n =$ the number of carbon atoms in an alkyl group) by colloidally dispersed zirconium phosphate (ZrP) was studied by spectrophotometry and electric dichroism. An $AO-C_n$ cation was bound to ZrP by releasing a proton in the phosphate group of ZrP. The electronic spectrum of bound $AO-C_n$ showed that the dye cations formed an aggregate on the polymer. The reduced linear dichroism of a bound dye molecule, ρ, was determined as a function of n: $\rho = 1.3$–1.0 for $n = 0$–2, while $\rho = -0.3$ to -0.4 for $n = 3$–9. The results implied that the bound structures of the dyes changed drastically when the length of the alkyl chain increased from 2 to 3. This suggested that the $AO-C_n$ cations with $n = 0$–2 oriented their transition moments, μ, in the same direction on a ZrP particle, while the $AO-C_n$ cations with $n = 3$–9 oriented their μ's randomly.

Introduction

Interaction of a chromophore of low molecular weight with a polyelectrolyte in solution has been the subject of numerous in-vestigations in recent years.[1-3] How does the difference in the structure of a small molecule affect its bound state on a polymer chain? How do the adsorbates interact with each other when the adsorption sites are located close to the polymer surface? Answers to these questions may give us a clue to the interaction of small molecules with each other when they form an aggregate on the polymer.

We have been studying alkyl chain effects on the dye–mac-romolecule interaction, using N-alkylated acridine orange cations as probe molecules. The macromolecules investigated are reversed micelles, poly(styrenesulfonic acid), montmorillonite, and sodium dodecanesulfonate micelles.[4-7]

In this paper, we report a study on the adsorption of a series of dye molecules by a colloidal form of zirconium phosphate (ZrP). A microcrystalline ZrP gel is a cation exchanger with a two-di-mensional layer structure.[8] Each crystallite has hydroxyl groups on its surface. ZrP might react with a dye molecule in various ways such as by electrostatic and hydrogen-bonding forces. The electronic spectra and electric dichroism were measured for this system to characterize the adsorption states of a molecules. As

a result, it was shown that the nature of the binding of a dye molecule changed drastically at a certain length of an alkyl chain.

Experimental Section

The γ form of zirconium phosphate (ZrP) gel was prepared by the method reported previously.[12] The gel was matured at 130 °C for 24 h. An aqueous mixture of a microcrystalline slurry was centrifuged at 3000 rpm for $^1/_2$ hour, and the precipitate was washed with distilled water. By this procedure, a part of the microcrystalline ZrP dispersed in the water phase. Combining the supernatant and the water, we dialyzed it through a cellulose tube (Union Carbide Corp.) for 3 days. The dialyzed suspension was used as a stock suspension of colloidal ZrP. The ZrP quantity in the suspension was determined by gravimetry after freezed-drying a known volume of the suspension. A series of N-alkyl acridine orange derivatives ($AO-C_n$; $n =$ the number of carbon atoms in an alkyl chain) were prepared as their chloride salts as described previously.[4] Electronic spectra were measured with a recording spectrophotometer, UVIDEC-430A (JEOL, Japan). Electric birefringence and electric dichroism were measured with an instrument as described elsewhere.[9] With this instrument, a square electric field pulse, 2 kV × 1 ms, was applied to a sus-pension. The intensity of the electric field was varied from 3 to 10 kV/cm by changing the distance between the electrodes. The electric birefringence was measured by monitoring the intensity of the light that passed through a polarizer, a sample, and an analyzer. The polarization angles of the polarizer and analyzer were set at 45° and 135° with respect to the electric field, re-spectively. Electric dichroism was measured by monitoring the transmittance change through a polarizer and a sample solution, in which the polarization angle of the polarizer was set at either 0° or 90° with respect to the electric field. The rate of the adsorption of a dye by ZrP was measured at 25 °C in a stop-ped-flow apparatus by monitoring the absorbance at 498 nm. The pH titration was performed at 20 °C with a Horiba pH meter

(1) Vitagiano, V.; Constantino, L.; Zagari, A. *J. Phys. Chem.* **1973,** *77,* 204.

(2) Hard, T.; Kearns, D. R. *J. Phys. Chem.* **1986,** *90,* 3437.

(3) Morawetz, H. *Science* **1988,** *240,* 172.

(4) Yamagishi, A.; Masui, T.; Watanabe, F. *J. Phys. Chem.* **1981,** *85,* 281.

(5) Yamagishi, A. *J. Phys. Chem.* **1981,** *85,* 3090.

(6) Yamagishi, A.; Watanabe, F. *J. Phys. Chem.* **1981,** *85,* 2129.

(7) Yamagishi, A. *J. Colloid Interface Sci.* **1982,** *82,* 468.

(8) Kijima, T.; Sekikawa, Y.; Ueno, S. *J. Inorg. Nucl. Chem.* **1981,** *43,* 849.

(9) Yamagishi, A. *J. Phys. Chem.* **1984,** *88,* 5709.

(10) Triot; Houssier, C. In *Polyelectrolyte;* Technomic: Westport, 1976; pp 43–90.

(11) Matsuoka, Y.; Yamaoka, K. *Bull. Chem. Soc. Jpn.* **1981,** *43,* 849.

(12) Yamanaka, S.; Tanaka, M. *J. Inorg. Nucl. Chem.* **1979,** *41,* 45.